PROCEEDINGS OF SPIE

SPIEDigitalLibrary.org/conference-proceedings-of-spie

Initial calibration activities and performance assessments of NOAA-20 VIIRS

Xiaoxiong Xiong, Hassan Oudrari, Jeff McIntire, Ning Lei, Kwofu Chiang, et al.

Xiaoxiong Xiong, Hassan Oudrari, Jeff McIntire, Ning Lei, Kwofu Chiang, Amit Angal, "Initial calibration activities and performance assessments of NOAA-20 VIIRS," Proc. SPIE 10781, Earth Observing Missions and Sensors: Development, Implementation, and Characterization V, 107810L (23 October 2018); doi: 10.1117/12.2326897

SPIE.

Event: SPIE Asia-Pacific Remote Sensing, 2018, Honolulu, Hawaii, United States

Initial Calibration Activities and Performance Assessments of NOAA-20 VIIRS

Xiaoxiong Xiong[1], Hassan Oudrari[2], Jeff McIntire[2], Ning Lei[2], Kwofu Chiang[2], and Amit Angal[2]

[1]*Sciences and Exploration Directorate, NASA GSFC, Greenbelt, MD 20771, USA*
[2]*Science Systems and Applications Inc., 10210 Greenbelt Rd, Lanham, MD 20706, USA*

ABSTRACT

The second VIIRS instrument was launched on-board the NOAA-20 (formerly JPSS-1) satellite on November 18, 2017. It was designed and built with the same performance requirements as the first VIIRS on-board the S-NPP launched on October 28, 2011. Currently, the NOAA-20 is orbiting the Earth in the same plane as the S-NPP but separated in time and space by 50 minutes. The VIIRS observations are made in 22 spectral bands, including a day-night band (DNB) that cover wavelengths from visible to long-wave infrared. The sensor's on-orbit calibration is provided by a set of on-board calibrators (OBCs), which include a solar diffuser (SD), a solar diffuser stability monitor (SDSM), and a blackbody (BB). After turn-on, the VIIRS instrument conducted a series of post-launch testing (PLT) and intensive calibration and validation (ICV) activities, including those performed via spacecraft maneuvers, designed to verify and establish instrument on-orbit calibration performance baseline. This paper provides an overview of NOAA-20 VIIRS ICV activities and an assessment of its initial on-orbit performance with a focus on several key calibration parameters, such as the detector response (or gain), dynamic range, and signal-to-noise ratio (SNR). Various issues identified and lessons learned from initial instrument operation and calibration are also discussed in support of long-term monitoring (LTM) of NOAA-20 VIIRS calibration and data quality.

Keywords: VIIRS, S-NPP, JPSS-1, NOAA-20, calibration, on-board calibrators, Moon

1. INTRODUCTION

The second Visible Infrared Imaging Radiometer Suite (VIIRS) instrument was launched on-board the NOAA-20 (designated JPSS-1 prior to launch) satellite on November 18, 2017[1]. It was built and characterized with the same design requirements as the first VIIRS instrument launched on October 28, 2011 on-board the S-NPP satellite. Currently, the NOAA-20 and S-NPP satellites are orbiting the Earth in the same plane (1:30 PM local equatorial crossing time, ascending node), with NOAA-20 leading SNPP by a half orbit, or ~50 minutes. The JPSS-1 is the first in a series of NOAA's four next-generation operational polar-orbiting weather satellites that provide scientists and weather forecasters with global measurements of the Earth's terrestrial, oceanic, and atmospheric conditions through 2038 using a set of complementary sensors (both passive and active) that cover a wide spectral range. The next satellite, JPSS-2, is currently scheduled to launch in 2022, followed by JPSS-3 and -4 in 2026 and 2031, respectively. In addition to S-NPP, the VIIRS instruments will fly on all JPSS satellites.

The VIIRS is a cross-track scanning radiometer, collecting data via a rotating telescope assembly (RTA), coupled with a two-sided half-angle mirror (HAM), in 22 spectral bands that include 14 reflective solar bands (RSB), 7 thermal emissive bands (TEB), and one panchromatic day-night band (DNB). The nominal

Earth Observing Missions and Sensors: Development, Implementation, and Characterization V
edited by Xiaoxiong Xiong, Toshiyoshi Kimura, Proc. of SPIE Vol. 10781, 107810L
 · doi: 10.1117/12.2326897

spatial resolutions at nadir of the moderate resolution bands (M1 – M16) and imaging bands (I1 – I5) are 750 m and 375 m, respectively[2-4]. Some key design parameters of the VIIRS spectral bands, such as their wavelengths, typical and maximum radiances or temperatures, and specified signal-to-noise ratios (SNR) or noise-equivalent temperature differences (NEdT), are listed in Table 1. M1-M5, M7, and M13 are the dual gain bands and the DNB observations use 3 gain stages (Low, Medium and High) to cover a very large dynamic range.

Table 1. Key design specifications of VIIRS spectral bands (radiance unit: $W/m^2/\mu m/sr$; temperature unit: K); *DNB L_{TYP} is defined as L_{MIN} (radiance unit: $W/m^2/sr$); **M11 L_{TYP} changed from 0.12 to 1.0 $W/m^2/\mu m/sr$ for JPSS VIIRS.

Band No.	Wavelengths (μm)	Gain	L_{TYP} or T_{TYP}	L_{MAX} or T_{MAX}	SNR or NEdT
DNB	0.500 - 0.900	H/M/L	3 e-5 (*)	200(*)	5
M1	0.402 - 0.422	High Low	44.9 155	135 615	352 316
M2	0.436 - 0.454	High Low	40 146	127 687	380 409
M3	0.478 - 0.498	High Low	32 123	107 702	416 414
M4	0.545 - 0.565	High Low	21 90	78 667	362 315
I1	0.600 - 0.680	Single	22	718	119
M5	0.662 - 0.682	High Low	10 68	59 651	242 360
M6	0.739 - 0.754	Single	9.6	41	199
I2	0.846 - 0.885	Single	25	349	150
M7	0.846 - 0.885	High Low	6.4 33.4	29 349	215 340
M8	1.230 - 1.250	Single	5.4	164.9	74
M9	1.371 - 1.386	Single	6	77.1	83
I3	1.580 - 1.640	Single	7.3	72.5	6
M10	1.580 - 1.640	Single	7.3	71.2	342
M11	2.225 - 2.275	Single	0.12**	31.8	10
I4	3.550 - 3.930	Single	270 (K)	353 (K)	2.5 (K)
M12	3.660 - 3.840	Single	270 (K)	353 (K)	0.396 (K)
M13	3.973 - 4.128	High Low	300 (K) 380 (K)	343 (K) 634 (K)	0.107 (K) 0.423 (K)
M14	8.400 - 8.700	Single	270 (K)	336 (K)	0.091 (K)
M15	10.263 - 11.263	Single	300 (K)	343 (K)	0.07 (K)
I5	10.500 - 12.400	Single	210 (K)	340 (K)	1.5 (K)
M16	11.538 - 12.488	Single	300 (K)	340 (K)	0.072 (K)

In addition to extensive pre-launch calibration and characterization made at different phases and environments, the VIIRS sensor carries a set of on-board calibrators (OBC) that include a solar diffuser (SD), a solar diffuser stability monitor (SDSM), and a blackbody (BB) for its on-orbit calibration in order to maintain data quality over its entire mission. A space view (SV) port, an extended sector of the Earth view port, enables the sensor to make deep space observations, correct for instrument background, and view the Moon[5]. Illustrated in Figure 1 are the VIIRS instrument scan cavity, its RTA and OBC, and the extended SV port. The NOAA-20 VIIRS post-launch activities, including those performed via spacecraft maneuvers, are described in its calibration and validation (Cal/Val) plan, which owes its heritage to the S-NPP VIIRS Cal/Val plan[6]. The post-launch period is a combination of three phases, the Post-Launch Test (PLT) or Early Orbit Instrument Checkout (EOC), the Intensive Calibration /Validation (ICV), and the Long-Term Monitoring (LTM).

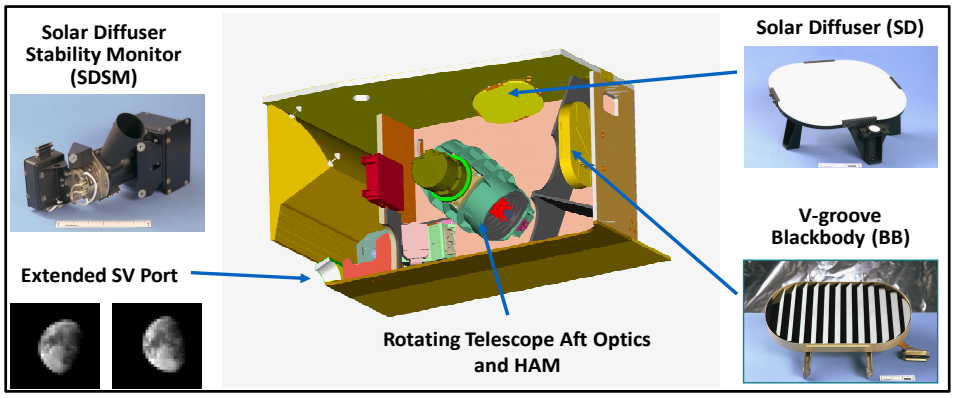

Figure 1. VIIRS instrument scan cavity and its on-board calibrators (OBC), including the space view (SV) port.

The PLT began as soon as the VIIRS instrument was turned on (November 28, 2017) and the raw data records (RDR) and sensor data records (SDR) were produced. The early released SDR were generated with at-launch calibration parameters and used by the calibration teams to perform initial qualitative and limited quantitative assessments of instrument and product performance, including identified anomalies and associated remediation strategies, and to assure that the SDR quality reaches the Beta maturity level (February 1, 2018). The second phase, ICV, began after the completion of the PLT phase, lasted about 4 months for NOAA-20 and included comprehensive and enhanced SDR evaluation and performance assessments that helped the SDR to reach the Provisional maturity (February 19, 2018) and Validated maturity (June 4, 2018).

This paper provides a brief description of NOAA-20 VIIRS on-orbit calibration and validation activities, especially those performed during PLT and ICV phases, and an overview of its calibration and characterization methodologies based on the use of its OBC and regularly scheduled lunar observations. It presents examples to demonstrate instrument on-orbit performance and issues identified and resolved. In general, the NOAA-20 VIIRS overall performance is as good as or better than its predecessor, S-NPP VIIRS, especially for the RSB. An initial ice buildup on the dewar widow of the LWIR focal plane assemblies (FPA) was identified shortly after opening the cryo-radiator door, which caused noticeable degradation of TEB responses (gains). This abnormal behavior was eliminated via a mid-mission outgassing (MMOG).

2. INITIAL ON-ORBIT OPERATION AND CALIBRATION ACTIVITIES

Shortly after launch, the NOAA-20 VIIRS instrument was turned on the first time on November 28, 2017 and started to perform initial activation and functional tests. The first Earth view image was captured immediately after opening the nadir aperture door on December 13, 2017. In addition to nominal use of its OBC, the VIIRS performed a number of special tests during the PLT and ICV phases to help assess the sensor at launch performance, including those conducted using data collected during spacecraft maneuvers. Listed in Table 2 are some key operation and calibration events during NOAA-20 VIIRS PLT and ICV.

Table 2. Key operation and calibration events during NOAA-20 VIIRS PLT and ICV

Date	Event
11/18/2017	JPSS-1 (NOAA-20) Launch
11/30/2017	SDSM 1st Measurement
12/13/2017	Nadir Aperture Door Open
12/18/2017	DNB 1st VROP Cal (New Moon)
12/29/2017	Lunar Cal 1st Roll Maneuver
12/29/2017	Safe Mode
01/03/2018	Cryo-radiator Door Open
01/10/2018	BB Warm-Up Cool-Down (Full)
01/17/2018	DNB VROP Cal (New Moon)
01/22/2018	BB Warm-Up Cool-Down (Short)
01/25/2018	Yaw Maneuvers
01/27/2018	Lunar Cal Roll Maneuver
01/31/2018	Deep Space Pitch Maneuver
02/02/2018	Safe Mode
02/15/2018	DNB VROP Cal (New Moon)
02/15/2018	Electronics Self-Test (LWIR Diagnosis)
02/16/2018	Raising BB Temperature (LWIR Diagnosis)
02/21/2018	Telescope Stow (LWIR Diagnosis)
02/26/2018	Lunar Cal Roll Maneuver
03/12/2018	Mid-Mission Outgassing

The spacecraft roll maneuvers are executed to facilitate the VIIRS lunar observations that play a critical role to monitor its RSB long-term calibration stability. The data sets collected during yaw maneuvers are used primarily to validate the SD bidirectional reflectance distribution function (BRDF) and solar attenuation screen (SAS) transmission, as well as the SDSM screen transmission. The pitch maneuver allows the sensor to view the deep space through its entire nadir aperture and provides useful data to characterize and validate the TEB response versus scan-angle (RVS) and also to validate and establish the DNB high gain offsets. Not just limited to PLT and ICV, the roll maneuvers are expected to be carried out through the entire LTM phase. The SD calibration is performed every orbit while the SDSM is currently operated on a daily basis. For

nominal operation, the on-board BB is controlled at a constant temperature at 292.5 K. In addition, a BB warm-up and cool-down (WUCD) operation was carried out quarterly during the ICV phase and its frequency has now been reduced to yearly for the future LTM phase.

Shortly after opening the cryo-radiator door, a noticeable degradation in the long-wave infrared (LWIR) detector responses or gains (in bands I5, M15 and M16) was observed. Following extensive reviews of instrument performance from pre-launch testing at different phases to on-orbit responses under various operating conditions and a number of diagnostic tests, such as the RTA stow and electronic self-test (see Table 2), the most probable cause of the degradation was believed to be due to the ice buildup on the dewar window of the LWIR FPA[7]. As to be shown later, a MMOG performed on March 12, 2018 was able to eliminate this abnormal behavior and restore the LWIR responses to their initial at-launch values.

Table 3. NOAA-20 VIIRS calibration and validation task categories

Category	Description	Number of Tasks
Functional Performance and Format (FPF)	FPF tasks involve evaluating instrument functions and verifying the correctness of data formats.	6
Calibration System Evaluation (CSE)	CSE tasks evaluate the performance of the onboard calibration system and update the calibration algorithm databases accordingly.	6
Image Quality Evaluation (IMG)	IMG tasks evaluate the quantitative and qualitative spatial performance characteristics of the instrument.	4
Radiometric Evaluation (RAD)	RAD tasks evaluate the radiometric performance of the data product algorithm, to address changes in the sensor characteristics to enhance data quality.	25
Geolocation/Geometric Evaluation (GEO)	GEO tasks evaluate the geolocation accuracy of the data product, while geometric tasks focus on the BBR, and MTF evaluation.	14
Performance and Telemetry Trending (PTT)	PTT tasks evaluate long-term changes in the performance of both the instrument and the data product.	9
Waiver verification (WAV)	WAV tasks focuses on the evaluation of the performance shortfalls underlying instrument waivers specific for N-20 VIIRS	8

The NOAA-20 VIIRS post-launch Cal/Val tasks are based on and modified from similar tasks performed for the S-NPP. A new category was added to address the sensor performance waivers (WAV). These tasks were grouped into seven categories as described in Table 3. While the instrument vendor has the overall responsibility to demonstrate that the instrument meets the performance requirements on orbit, the government calibration teams and their efforts have played a crucial role through the post-launch phase. Each task was assigned to at least one subject matter expert, and data analyses and findings were presented and reviewed daily, enabling a quick and high-quality assessment of sensor performance and development of necessary SDR algorithm changes to address issues identified in order to improve the existing data quality.

3. ON-ORBIT CALIBRATION METHODOLOGIES

Details of the VIIRS on-orbit calibration and characterization methodologies, including changes and improvements made in recent years, can be found in a number of references[5, 8-18]. Only a brief description is provided in this section to support the assessment of instrument on-orbit performance to be discussed in the next section.

As shown in Figure 1, the SD observations allow the RSB on-orbit calibration coefficients (or the F-factors) to be derived each orbit when it is illuminated by the Sun over the south pole region. Placed in front of the SD is a fixed attenuation screen. As a result, the RSB calibration is reflectance-based with traceability tied to the SD BRDF, which was characterized pre-launch by the instrument vendor. Similarly, the transmission of the attenuation screen was also measured pre-launch over a range of illumination angles. In this approach, the quality of SD BRDF and its screen transmission measurements has a direct impact on the RSB calibration accuracy. Like all RSB, the DNB low gain stage calibration is also performed using the SD and SDSM calibration system. It requires, however, SD observations made over multiple orbits to derive a complete set of DNB gains in order to cover all the aggregation modes. At the same time, the DNB mid gain and high gain stages (MGS and HGS) can be calibrated via ratios of the LGS to MGS and MGS to HGS, respectively[8-9].

Changes in SD BRDF due to on-orbit exposure of the solar UV radiation are frequently tracked by the on-board SDSM. It is essentially a ratioing radiometer that has 8 filtered detectors, covering wavelengths from 0.41 to 0.93 μm, embedded in a solar integration sphere. The SDSM determines the SD degradation (or H-factors) by referencing its SD view observations against the Sun view observations made through a separate attenuation screen. For the short-wavelength infrared (SWIR) that is not covered directly by the SDSM, the SD degradation can be computed using a degradation model with its parameters derived from the SD degradation at the visible (VIS) and near-infrared (NIR) wavelengths[10].

The F-factors are the scaling factors to the pre-launch calibration coefficients. For the RSB, they are determined by comparing the expected radiance off the SD panel with that retrieved from detector responses (SV background subtracted) using the pre-launch calibration coefficients. Similarly, for the TEB, the F-factors are computed by comparing the expected path radiance when the sensor views the on-board BB with that retrieved from detector responses to the BB using the pre-launch calibration coefficients. Unlike RSB, the TEB calibration is performed on a scan-by-scan basis. In addition to BB, a number of emissive sources along the optical path, such as instrument background (fixed optics), the RTA, and HAM, need to be taken into account in TEB calibration algorithms. Some of the terms vary with the scan angle of the RTA.

The Moon can also be used as a calibration target, especially for monitoring the RSB long-term calibration stability. Using the same calibration approach as SD, one can derive “equivalent” F-factors using lunar observations. In this case, the predicted lunar irradiance from the ROLO is used to correct for the lunar viewing geometry differences[11]. By comparing the long-term trending of the F-factors derived from the SD observations with that from the lunar observations, one can accurately determine the SD degradation at all RSB wavelengths. NOAA-20 VIIRS lunar observations are scheduled and implemented exactly the same way as S-NPP, including the spacecraft roll angle constraints, the lunar phase angles (-51.5° to -50.5°). VIIRS lunar observations can also be used to monitor on-orbit changes in band-to-band registration (BBR)[12].

4. NOAA-20 VIIRS PERFORMANCE ASSESSMENTS

The left panel of Figure 2 shows the NOAA-20 VIIRS SDSM detector gains (normalized to the launch date) as estimated from its Sun-view responses, with corrections for the SDSM screen transmission function and the distance between the Sun and sensor. The on-orbit SDSM screen transmission function, initially derived from yaw maneuvers, was further enhanced using supplemental on-orbit measurements to achieve a better coverage of various view geometries. The SDSM detector with the longest wavelength (0.93 μm) has experienced the largest gain decrease. This wavelength-dependent detector gain change is similar to S-NPP VIIRS. The root cause of this wavelength dependent detector gain decrease is most likely due to the radiation damage to the detectors by the high energy particles in the space environment[19].

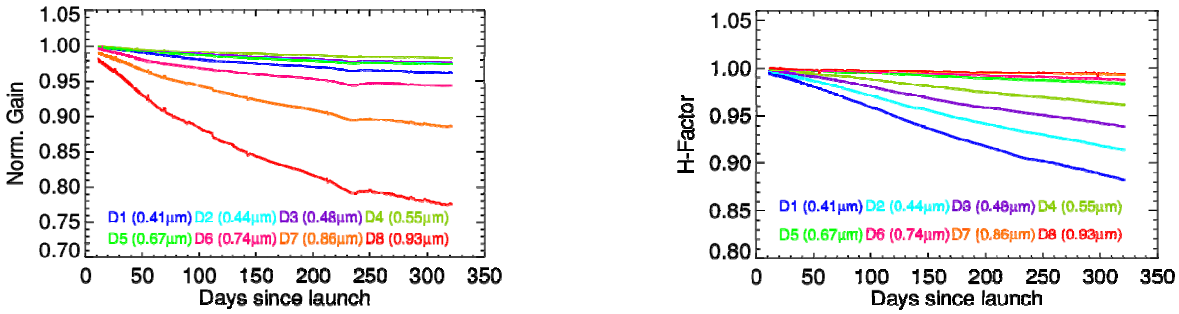

Figure 2. NOAA-20 VIIRS normalized SDSM detector gains (left) and its SD degradation or H-Factors (right)

The right panel of Figure 2 illustrates the SD on-orbit degradation (or H-Factors) as measured by the SDSM. Similar to S-NPP, the SD degrades more at shorter wavelengths. As described earlier, the SDSM is a ratioing radiometer and determines the SD on-orbit degradation by comparing its SD view responses with the the Sun view responses. The wavelength dependent behavior of the SD degradation and SDSM detector gain change of both VIIRS is very similar to that observed in MODIS instruments[20].

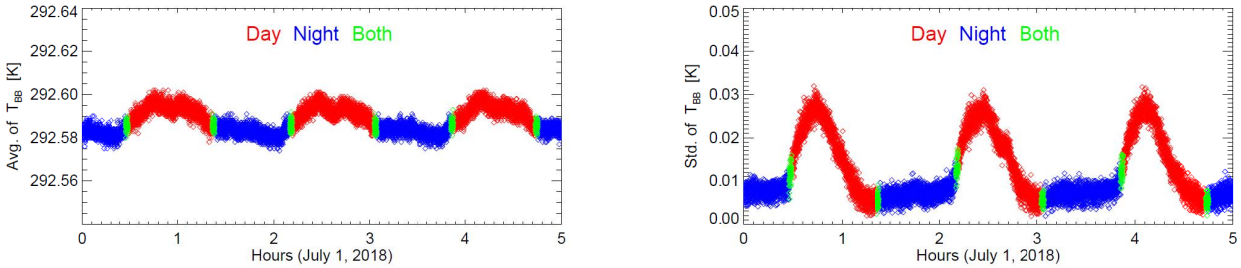

Figure 3. BB scan-by-scan short-term (3 orbits) stability (left) and its uniformity or standard deviation among 6 thermistors (right).

The on-board BB serves as the TEB calibration source and is nominally controlled at 292.5 K. The BB temperature is measured each scan by 6 thermistors. These thermistors are calibrated pre-launch with reference to the NIST temperature standard. In addition to the temperature measurement accuracy of each individual thermistor, the BB temperature uniformity, expressed by the standard deviation of the temperatures recorded by all 6 thermistors, is also a contributor to the TEB calibration quality. Figure 3 serves as a demonstration of BB temperature short-term stability and uniformity for NOAA-20 VIIRS using data from 3 consecutive orbits. The average temperatures show small variations of less than 25 mK between

the daytime and nighttime orbits and their standard deviations are less than 30 mK, which is the BB source uniformity design requirement. As expected the nighttime orbits show better stability and uniformity than the daytime orbits. During BB WUCD, the BB temperature uniformity slightly suffers due to changes of BB temperatures, more during WU process than the CD process.

Shown in Figure 4 are the normalized gains (1/F-factors) of the VIS and NIR bands, which are derived from both the SD and lunar observations. Clearly, the on-orbit changes in RSB gains to date have been very small, including the SWIR bands (not shown). M1 is the shortest wavelength (0.41 μm) band and has experienced the largest change at approximately 1.0%. There are some small but noticeable deviations between the SD and lunar gain trends presented in Figure 4. It is believed some of the differences are due to lunar view geometry differences that have not completely accounted for in the existing ROLO model. This behavior, also noticed in S-NPP VIIRS SD and lunar gain trends, can be removed via an empirical correction that is wavelength and lunar view geometry dependent. The long-term agreement between the SD and lunar gains will be carefully monitored and their differences can be used to correct SD degradations (H-factors) used in SD F-factors. Compared to S-NPP, NOAA-20 VIIRS RSB are much stable. The mirror contamination issue existed in S-NPP that led to large changes in some NIR and SWIR spectral bands is not present in NOAA-20 VIIRS[21-23].

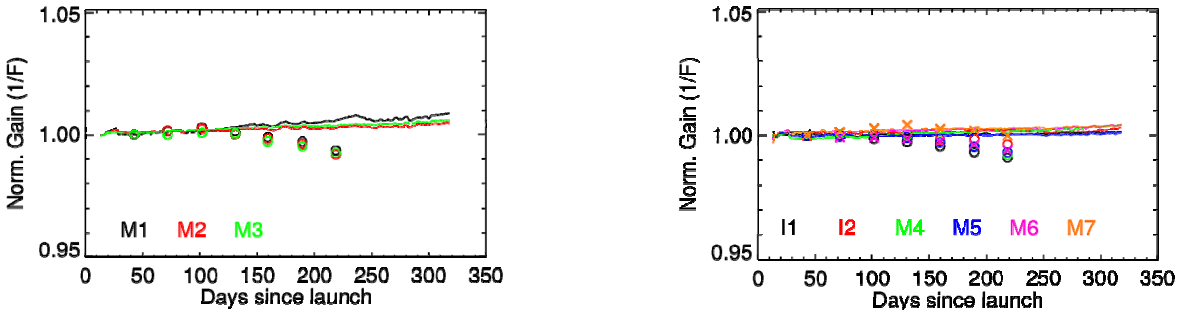

Figure 4. Normalized gains (inverse of F-factors) for NOAA-20 VIIRS VIS and NIR bands (HAM A, band average). Solid lines are SD measurements and symbols are lunar measurements.

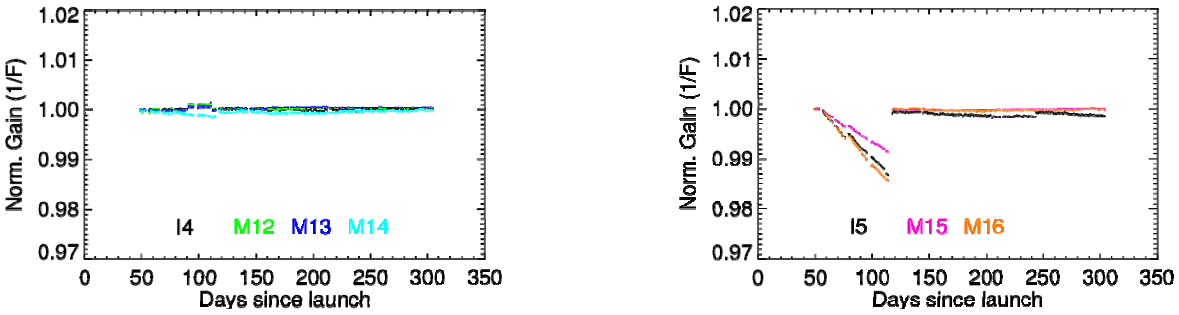

Figure 5. Normalized gains (inverse of F-factors) for NOAA-20 VIIRS MWIR and LWIR bands (HAM-A, band averaged).

Similar to RSB, the normalized gains (inverse of the F-factors) are used to assess the TEB on-orbit performance, in terms of their calibration stability. As illustrated in Figure 5, the changes in MWIR gains have been extremely small since launch. However, there was a gradual degradation or decrease in the LWIR

gains at the mission beginning. As discussed earlier, this was caused by the initial ice buildup on the LWIR FPA dewar window. A MMOG was conducted after identifying the root cause, resulting in an improved performance with the LWIR gains returning to the at-launch values. Since then, all TEB responses have been very stable and their performance has been very similar to S-NPP VIIRS TEB. After nearly 7 years, the S-NPP TEB gain change remains within 0.5% with the exception of I5, which has a gain change of about 1.8%.

In addition to spectral band responses, the detector noise characterization has been monitored since launch on a regular basis. For RSB, the SNR are routinely monitored using SD observations at different illumination conditions or signal levels. Similarly, data collected from BB WUCD allow TEB NEdT to be characterized at different temperature or radiance levels. Results illustrated in Figure 6 are the ratios of measured SNR (or NEdT) to specified SNR_{SPEC} (or $NEdT_{SPEC}$), including those from both pre-launch and on-orbit measurements. For comparison purposes, the measured SNR (or NEdT) are scaled (via interpolation or extrapolation) to their typical radiance (or temperature) values. $SNR/SNR_{SPEC} > 1$ (or $NEdT/NEdT_{SPEC} < 1$) indicates the performance is better than the specified requirements. As demonstrated in Figure 6, both RSB and TEB have exhibited excellent noise performance, from launch to present.

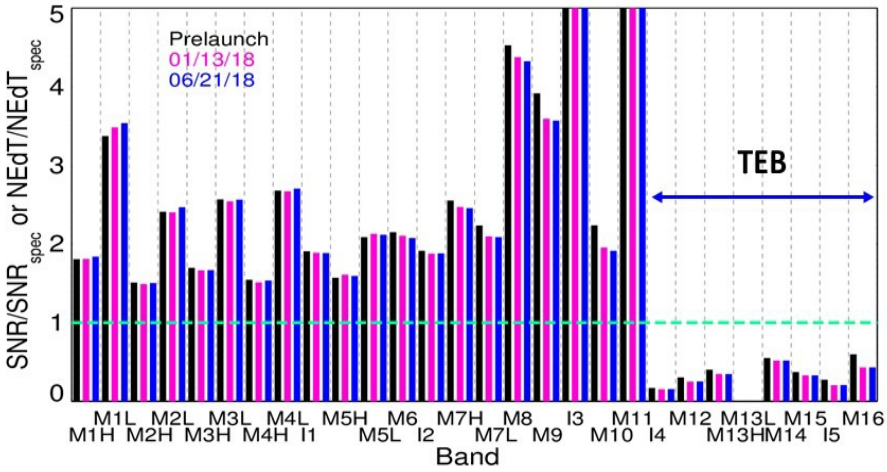

Figure 6 NOAA-20 VIIRS RSB SNR and TEB NEdT performance (results normalized to specified requirements)

The spectral band radiometric dynamic ranges were verified right after launch to ensure compliance with sensor requirements, and to compare to the values derived from pre-launch thermal vacuum testing. These results are shown in Figure 7 for both RSB and TEB, as well as a comparison with the S-NPP performance derived right after S-NPP launch. All RSB are meeting their maximum radiance requirements except for M8 with its saturation radiance reaching only 72% of the maximum radiance requirement. This is expected from pre-launch testing. While I3 was marginally noncompliant in the pre-launch testing, its post-launch values are in compliance with small margins. S-NPP showed non-compliance for both bands M8 and I3 before and after launch. Similar to S-NPP, the dynamic ranges of NOAA-20 TEB are in compliance with the requirements.

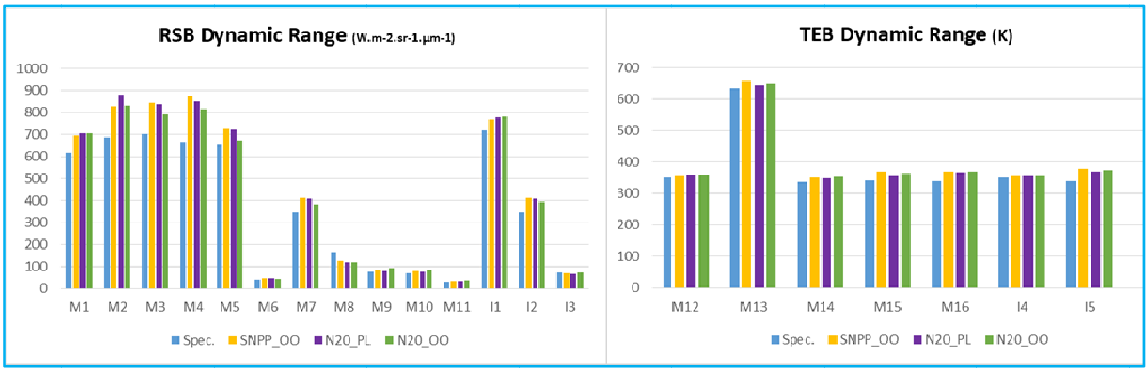

Figure 7 VIIRS dynamic range specification and performance (RSB radiance in W/m^2/μm/sr and TEB temperature in K): S-NPP on-orbit (SNPP_OO), NOAA-20 pre-launch (N20_PL) and on-orbit (N20_OO).

Like RSB, the NOAA-20 VIIRS DNB responses have also been very stable from launch to present in all three gain stages. The DNB high gain stray light problem in S-NPP also exists in NOAA-20, but to a lesser extent. A similar correction approach is applied to both S-NPP and NOAA-20[24]. In general, the correction has been very effective as illustrated in Figure 8. The left panel is a DNB nighttime image over North America (from data granule 07:44:45, 07/13/2018) before the stray light correction is applied. A large area of the image is severely impacted by the stray light contamination. The right panel is the same image with stray light correction applied and shows significant improvements for the image quality. As an effort to minimize the nonlinearity in NOAA-20 DNB high aggregation modes, a modified aggregation configuration (option 21) was proposed and implemented, which resulted in an extended swath and reduced spatial resolutions at the edge of scan. The stray light contamination in the extended area (not shown here) is much larger than other areas and, therefore, requires special attention when applying the stray light correction, including their correction coefficients.

Figure 8. NOAA-20 VIIRS DNB nighttime image over North America (from granule 07:44:45, 07/13/2018). Left (Right): before (after) stray light correction is applied

In addition to radiometric calibration for the RSB, lunar observations can also be used to characterize the band-to-band registration (BBR). This approach was first developed and applied to MODIS instruments with results verified by a special on-board calibrator of MODIS that can perform spectral and spatial characterization. It was later adopted and used for SNPP VIIRS[12]. Most TEB responses saturate when viewing the Moon. As a result, only the RSB BBR are characterized using this approach.

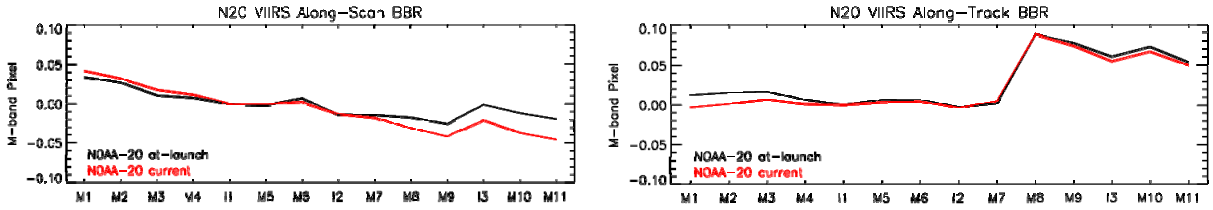

Figure 9. NOAA-20 VIIRS along-scan (left) and along-track (right) BBR from lunar measurements. At launch values are shown in black and current values (June 2018) are shown in red.

Figure 9 shows the along-scan and along-track BBR for NOAA-20 using the initial and latest lunar observations. Since launch, the BBR have been extremely stable. Compared to pre-launch, however, there is a small shift (less than 10% of the M-pixel size) of the along-track BBR between the bands on warm and cold focal FPA. Another application of lunar observations is to evaluate calibration consistency between two sensors, such as S-NPP and NOAA-20 VIIRS or VIIRS and MODIS. Preliminary results show that the calibration differences between the two VIIRS RSB are about 2-3% when using the current operational F-factors. With future calibration improvements and updates to the calibration coefficients, the calibration differences need to be re-evaluated.

Apart from those illustrated above, a number of other tasks were also performed in support of the ICV phase covering aspects of VIIRS data format, instrument functionality, calibrator data quality, and image analysis. Some of these tasks were only performed early in the mission while some are regularly conducted as part of the instrument LTM activities. In terms of the instrument functionality, ICV tasks investigated the following: detector operability and noise performance, dual gain band and DNB transition verification, in-scan aggregation and bow-tie deletion verification, DCR performance, dual gain anomaly analysis, DNB offset verification, and histogram verification. All tasks reported the instrument as functioning within expectations. Calibrator data quality was verified by the following tasks: BB temperature uniformity, SD and SDSM view data quality checks, and moon in space view verification. Again, the calibrator data was verified to provide high quality on-orbit calibration for the VIIRS instrument. Image quality analysis using Earth view scenes was performed to check for the following: echoes, ghosts, crosstalk, striping, glints, and saturation. NOAA-20 showed comparable levels of image quality to SNPP VIIRS.

In addition, data from two sets of maneuvers that were performed only once at the mission beginning were analyzed: a series of yaw maneuvers and a pitch over maneuver. The yaw maneuver analysis was performed to verify and update the SD BRDF and attenuation screen vignetting functions. This was successful in significantly improving the H-factor trending, although further updates were required to fully characterize the SD degradation factor. The pitch maneuver verified the TEB RVS characterized prior to launch and provided a better dark reference (uncontaminated by air glow) for the DNB offset.

5. SUMMARY

This paper has provided a brief description of the NOAA-20 VIIRS on-orbit calibration activities and performance of the first 9 months. As illustrated, the NOAA-20 RSB on-orbit responses have been very stable since launch. The mirror coating contamination problem, which led to a large degradation in S-NPP

NIR and SWIR responses, is not present in NOAA-20. An early ice buildup problem affecting the performance of TEB LWIR was identified and removed by a mid-mission outgassing, resulting in improved TEB performance. Compared to S-NPP, the DNB stray light impact is slightly smaller in NOAA-20 and the same correction approach is being applied effectively. Lunar observations have been used for a number of calibration and characterization tasks. Comprehensive investigation of all the tasks performed during the ICV performance checkout showed that the NOAA-20 VIIRS instrument is performing as expected based on its pre-launch characterization and that it is showing comparable (and in many cases improved) performance relative to SNPP VIIRS.

ACKNOWLEDGEMENTS

The authors would like to acknowledge other members of the VIIRS Characterization Support Team (VCST) for their contributions and support.

REFERENCES

1. Xiong, X., C. Cao, N. Lei, K. Chiang, A. Angal, Y. Li, S. Blonski, W. Wang, and T. Choi, "Early Results from NOAA-20 (JPSS-1) VIIRS On-orbit Calibration and Characterization," Proceedings of IGARSS 2018.
2. Schueler, C. F., E. Clement, P. Ardanuy, C. Welsh, F. De Luccia, and H. Swenson, "NPOESS VIIRS sensor design overview," Proc. SPIE, 4483, 11-23, 2002
3. Murphy, R.P., P. E. Ardanuy, F. Deluccia, J. E. Clement, and C. Schueler, "The visible infrared imaging radiometer suite, Earth Science Satellite Remote Sensing," vol. 1, New York, USA: Springer-Verlag, pp. 199–223, 2006
4. Cao, C., F. Deluccia, X. Xiong, R. Wolfe, and F. Weng, "Early On-orbit Performance of the Visible Infrared Imaging Radiometer Suite (VIIRS) onboard the Suomi National Polar-orbiting Partnership (S-NPP) Satellite," IEEE Trans. Geosci. Remote Sens., vol. 52, no.2, pp.1142-1156, doi: 10.1109/TGRS.2013.2247768, 2014
5. Xiong X., J. Butler, K. Chiang, B. Efremova, J. Fulbright, N. Lei, J. McIntire, H. Oudrari, J. Sun, Z. Wang, and A. Wu, "VIIRS On-orbit Calibration Methodology and Performance," JGR Vol. 119, Issue 9, pp 5065-5078, 2014
6. NOAA Joint Polar Satellite System (JPSS) VIIRS Calibration/Validation Plan Version 1.0, December 31, 2015
7. Johnson, E., A. Lovelace, J. Higgins-Montoya, J. Yee, "JPSS-1 VIIRS emissive band radiometric performance trending," Proc. SPIE, 10785, 1078515, 2018
8. Lee, S., J. McIntire, H. Oudrari, T. Schwarting, X. Xiong, "A New Method for Suomi-NPP SIIRS Day-Night Band On-Orbit Radiometric Calibration," IEEE Trans. Geosci. Remote Sens., vol. 53, 324–334, 2015
9. Chen, H., X. Xiong, C. Sun, X. Chen and K. Chiang, "Suomi-NPP VIIRS day-night band on-orbit calibration and performance," Journal of Applied Remote Sensing, vol 11 (3), 36019, 2017
10. Lei, N., and X. Xiong, "Suomi NPP VIIRS Solar Diffuser BRDF Degradation Factor at Short-Wave Infrared Band Wavelengths," IEEE Trans. Geosci. Remote Sens., vol 54, issue 10, pp 6212-6216, 2016
11. Xiong, X., J. Sun, J. Fulbright, Z. Wang, and J. Butler, "Lunar Calibration and Performance for S-NPP VIIRS Reflective Solar Bands," IEEE Trans. Geosci. Remote Sens., vol 54, 1052-1061, 2015

12. Wang, Z., X. Xiong, Y. Li, “Update of VIIRS on-orbit spatial parameters characterized with the Moon,” IEEE Trans. Geosci. Remote Sens., vol. 53, 5486–5494, 2015
13. Fulbright, J., N. Lei, B. Efremova, and X. Xiong, “Suomi-NPP VIIRS Solar Diffuser Stability Monitor Performance,” IEEE Trans. Geosci. Remote Sens., vol. 54, 631-639, 2016, DOI: 10.1109/TGRS.2015.2441558
14. Efremova, B., J. Mcintire, D. Moyer, A. Wu, and X. Xiong, “S-NPP VIIRS thermal emissive bands on-orbit calibration and performance,” Journal of Geophysical Research, Volume 119, Issue 18, pp 10859-10875, 2014
15. Lei, N., X. Xiong, and B. Guenther, "Modeling the Detector Radiometric Gains of the Suomi NPP VIIRS Reflective Solar Bands," IEEE Transactions on Geoscience and Remote Sensing, vol.53(3), 1565-1573, 2015.
16. Cao, C., W. Wang, S. Blonski, B. Zhang, “Radiometric traceability diagnosis and bias correction for the Suomi NPP VIIRS long□wave infrared channels during blackbody unsteady states,” J. Geophys. Res. Atmos., 122, 5285–5297, 2017
17. Sun, J. and M. Wang, "Radiometric calibration of the Visible Infrared Imaging Radiometer Suite reflective solar bands with robust characterizations and hybrid calibration coefficients," Appl. Opt., 54, 9331-9342, 2015.
18. Lei, N., X. Chen and X. Xiong, “Determination of the SNPP VIIRS SDSM Screen Relative Transmittance From Both Yaw Maneuver and Regular On-Orbit Data,” IEEE Transactions on Geoscience and Remote Sensing, vol. 54, issue 3, pp. 1390-1398, 2016.
19. Xiong, X., A. Angal, J. Sun, T. Choi, and E. Johnson, “On-orbit performance of MODIS solar diffuser stability monitor.” Journal of Applied Remote Sensing, vol 8, 083514, 2014.
20. Xiong, X., J. Fulbright, A. Angal, Z. Wang, X. Geng, and J. Butler, "Assessment of MODIS and VIIRS solar diffuser on-orbit degradation," Proc. SPIE 9607, 96071T, 2015.
21. De Luccia, F., D. Moyer, E. Johnson, K. Rausch, K., N. Lei, K. Chiang, X. Xiong, J. Fulbright, E. Hass, and G. Iona, “Discovery and characterization of on-orbit degradation of the Visible Infrared Imaging Radiometer Suite (VIIRS) Rotating Telescope Assembly (RTA),” Proc. SPIE, vol. 8510, 85101A, 2012
22. Barrie, J., P. D. Fuqua, M. J. Meshishnek, M. Ciofalo, C. Chu, J. Chaney, R.Moision, and L. Graziani, “Root cause determination of on-orbit degradation of the VIIRS rotating telescope assembly,” Proc. SPIE, 8510, 851009, 2012
23. Iona, G., J. J. Butler, B. Guenther, E. H. Johnson, B. Kennedy, C. J. Kent, R. W. Lambeck, E. Waluschka, and X. Xiong, “VIIRS on-orbit optical anomaly: Investigation, analysis, root cause determination and lessons learned,” Proc. SPIE, 8510, 85101C, 2012
24. Chen, H., H. Oudrari, C. Sun, T. Schwarting, X. Xiong, “An early assessment of the JPSS-1/NOAA-20 VIIRS day-night band on-orbit calibration and performance,” Proc. SPIE, 10785, 1078517, 2018